

Mapping the Surface Heat of Luminescent Solar Concentrators

 Yujian Sun ¹, Yongcao Zhang ² and Yilin Li ^{3,*} 
¹ Department of Earth and Environmental Engineering, Columbia University, New York, NY 10027, USA; ys3495@columbia.edu

² Physical Sciences and Engineering Division, King Abdullah University of Science and Technology, Jeddah 23955, United Arab Emirates; yongcaozhang@gmail.com

³ Department of Chemical and Biomolecular Engineering, Rice University, Houston, TX 77005, USA

* Correspondence: yilinli@rice.edu

Abstract: Luminescent solar concentrators (LSCs) have been widely studied for their potential application as building-integrated photovoltaics (BIPV). While numerous efforts have been made to improve the performance, the photothermal (PT) properties of LSCs are rarely investigated. In this report, we studied the PT properties of an LSC with a power conversion efficiency (PCE) of 3.27% and a concentration ratio of 1.42. The results showed that the total PT power of the LSC was 13.2 W, and the heat was concentrated on the edge of the luminescent waveguide with a high heat power density of over 200 W m⁻².

Keywords: luminescent solar concentrator; photovoltaic; photothermal; ray-tracing simulation



Citation: Sun, Y.; Zhang, Y.; Li, Y. Mapping the Surface Heat of Luminescent Solar Concentrators. *Optics* **2021**, *2*, 259–265. <https://doi.org/10.3390/opt2040024>

Academic Editor: Diogo Canavarro

Received: 7 October 2021

Accepted: 10 November 2021

Published: 16 November 2021

Publisher's Note: MDPI stays neutral with regard to jurisdictional claims in published maps and institutional affiliations.



Copyright: © 2021 by the authors. Licensee MDPI, Basel, Switzerland. This article is an open access article distributed under the terms and conditions of the Creative Commons Attribution (CC BY) license (<https://creativecommons.org/licenses/by/4.0/>).

1. Introduction

The practical integration of conventional solar panels with architectures such as buildings and other physical structures remains challengeable due to the design limitations of conventional solar panels such as shape, color, and transparency [1–3]. The approach of luminescent solar concentrators (LSCs) as building-integrated photovoltaics (BIPV) is considered promising for circumventing the practical issues of conventional solar panels because solar cells are placed on the edge of the luminescent waveguide in LSCs [4–6]. With this design, the shape of LSCs can be arbitrary, and the color and transparency can be tuned by the properties of the luminophores in the waveguide [7–9]. The operational mechanism of LSCs is shown in Figure 1. A fraction of sunlight is absorbed by the luminophores and converted to luminescent light, which follows the successive total internal reflection (TIR) and travels to the solar cells that are placed on the edge of the waveguide. Studies have shown that LSCs can be operated under different light conditions [10,11] and utilized in other areas beyond architectures [12].

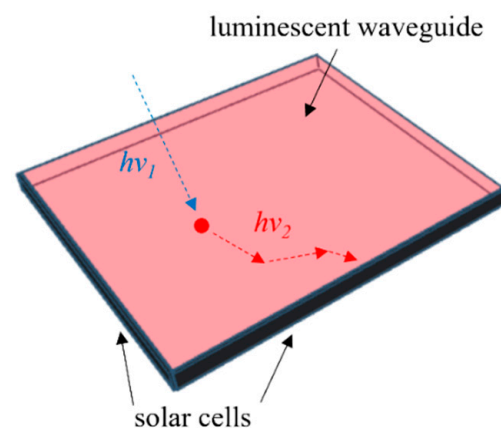


Figure 1. The operational mechanism of luminescent solar concentrators (LSCs).

In recent years, the research focus on LSCs has mainly been on improving the photovoltaic (PV) performance of the devices, particularly the power conversion efficiency (PCE) [13–15], through developing novel luminophores [16–18] and optical techniques [19–21]. These approaches mainly focused on improving the photon collecting and transporting efficiencies of the LSCs, while little attention was paid to making use of the photon energy loss. In LSCs, a significant amount of photon energy loss was through the photothermal (PT) process. Therefore, it is of great importance to study the PT properties of LSCs and find solutions to utilize the PT energy. Recently, our team performed a preliminary investigation of the PT properties of LSCs through Monte Carlo ray-tracing simulations [22]. We showed that the PCE could also be improved through the utilization of PT energy by thermoelectric devices that have been widely developed [23–25]. In this report, we further studied the PT properties of LSCs through the surface heat map. The results indicated that the heat concentrated on the edge of the luminescent waveguide, suggesting that LSCs could also be applied as PT energy concentrators. This study would guide the design of novel LSCs that include PT energy utilization.

2. Experimental Section

2.1. Device Fabrication

In this study, we fabricated an LSC with dimensions of 200 mm × 200 mm × 5 mm. The fabrication procedure occurred according to our previous reports [26–28]. We used 4-(dicyanomethylene)-2-*tert*-butyl-6-(1,1,7,7-tetramethyljulolidin-4-yl-vinyl)-4*H*-pyran (DCJTb) as the luminophores [29,30] in the waveguide and attached gallium arsenide (GaAs) solar cells to the edge of the waveguide [31]. The concentration of DCJTb was 60 ppm. The dimensions of the waveguide were 200 mm × 200 mm × 5 mm, and those of the solar cells were 200 mm × 5 mm. All four edges of the waveguide were covered by the solar cells. The solar cells were connected in parallel.

2.2. Device Characterization

The absorption and emission spectra of DCJTb in the waveguide were measured using a Varian Cary 5000 UV-visible-NIR spectrometer and an ISS PC1 photon-counting spectrofluorometer, respectively. The photoluminescence quantum yield (PLQY) of DCJTb was measured using an integrating sphere connected to a Hamamatsu C9920-12 external quantum efficiency (EQE) measurement system. The PV properties of the solar cells and the LSC were measured under ambient conditions [32]. The I–V curves of the solar cells and the LSC were measured with a Keithley 2401 Sourcemeter. The EQE of the solar cells and the LSC were measured on an Enlitech QE-R3011 system. The AM1.5G sunlight (1000 W m⁻²) was provided by an OAI class AAA solar simulator.

2.3. Ray-Tracing Simulation

The ray-tracing simulation was performed using a commercial Monte Carlo ray-tracing service provided by Solarathlon. Details about the simulation cannot be disclosed according to the service policy. The service was customized to obtain the internal and surface heat maps of the luminescent waveguide.

3. Results and Discussion

3.1. Spectroscopic and PV Properties

We first characterized the spectroscopic properties of DCJTb in the LSC and the PV properties of the GaAs solar cells and the LSC, which were recommended by the LSC research community in a recent paper [33]. Figure 2a shows the normalized absorption and emission spectra of DCJTb in the LSC. The absorption spectrum of DCJTb was maximized at 494 nm and covered the wavelength range until 600 nm. The emission spectrum of DCJTb was maximized at 598 nm, and the Stokes shift was 104 nm. Figure 2b depicts the results for the PLQY of DCJTb in the LSC. PLQY was defined as the ratio between the number of emitted photons (N_{em}) and the number of absorbed photons (N_{abs}), which

was 0.80 [34]. The PV properties of the GaAs solar cells are shown in Figure 2c,d. For four parallelly connected solar cells with a total area of 0.004 m^2 ($= 200 \text{ mm} \times 5 \text{ mm} \times 4$), the I-V measurement provided a short-circuit current (I_{sc}) of 1.11 A, an open-circuit voltage (V_{oc}) of 1.03 V, and a fill factor (FF) of 0.80, which led to a maximum electric power (P_{max}) of 0.92 W and a PCE of 23%. The external quantum efficiency (EQE) of the GaAs solar cells exhibited a strong spectral response of over 0.85 from 500 nm to 850 nm. The integrated short-circuit current density (J_{sc}) (i.e., integration of EQE with AM1.5G solar spectrum along the wavelength) was 278.32 A m^{-2} , which was consistent with that from the I-V measurement ($277.5 \text{ A m}^{-2} = 1.11 \text{ A}/0.004 \text{ m}^2$). The PV properties of the LSC are depicted in Figure 2e,f. When the GaAs solar cells were attached to the luminescent waveguide, the resulting LSC with an area of 0.04 m^2 ($= 200 \text{ mm} \times 200 \text{ mm}$) exhibited an I_{sc} of 1.54 A, a V_{oc} of 1.05 V, and an FF of 0.81, which led to a P_{max} of 1.31 W and a PCE of 3.27%. The concentration ratio, defined as the electrical power of the LSC relative to that of the solar cells, was 1.42 ($= 1.31 \text{ W}/0.92 \text{ W}$), which indicated that the luminescent waveguide was a light concentrator for the GaAs solar cells. The lower PCE of the LSC compared with the PCE of the GaAs solar cells was due to the low J_{sc} of the LSC ($38.5 \text{ A m}^{-2} = 1.54 \text{ A}/0.04 \text{ m}^2$). The EQE of the LSC before 600 nm was due to the absorption of DCJTb, while that after 600 nm was due to the scattering effects in the luminescent waveguide [35–37]. The integrated J_{sc} of the LSC was 38.26 A m^{-2} . A Monte Carlo ray-tracing simulation was performed to obtain the PCE of the LSC. The simulation provided a PCE of 3.3%, which was in good agreement with the experimental value (3.27%).

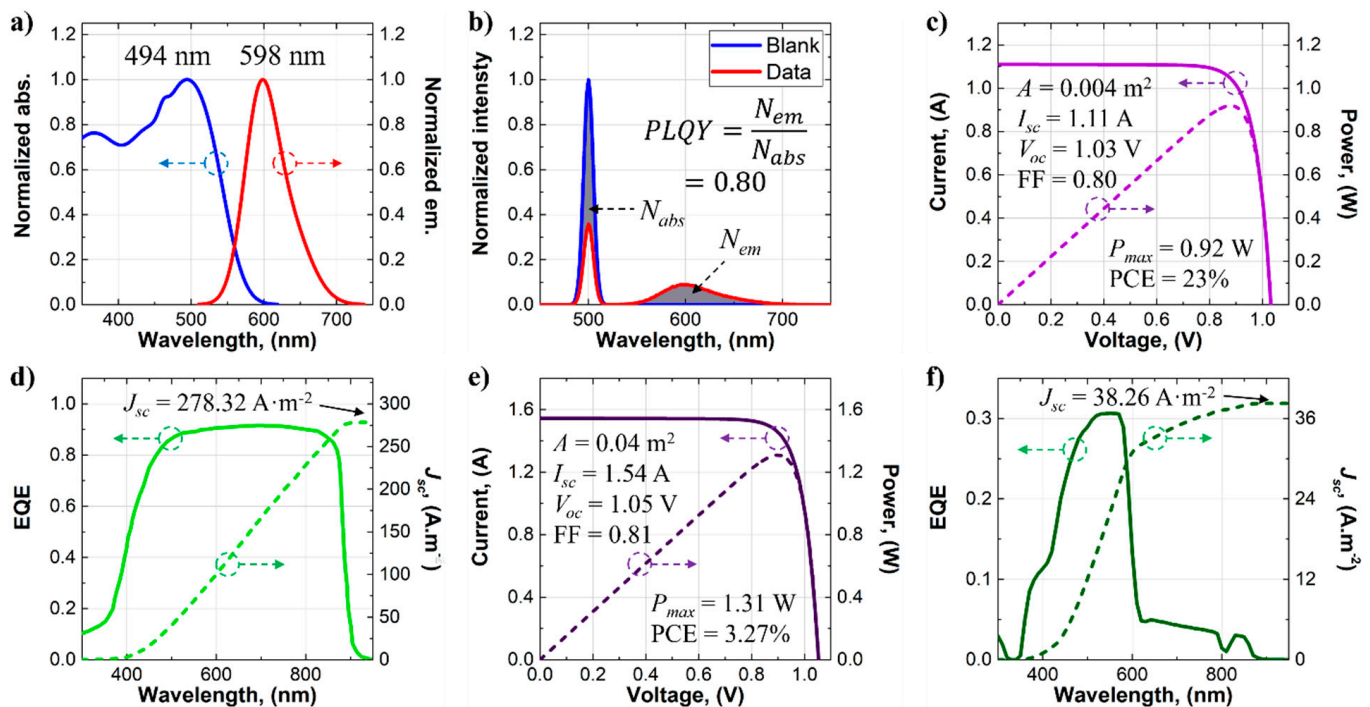


Figure 2. (a) Normalized absorption and emission spectra and (b) results for the PLQY of DCJTb in the LSC. Results for the (c) I-V and (d) EQE measurements of the GaAs solar cells. Results for (e) the I-V and (f) the EQE measurements of the LSC.

3.2. PT Properties

The PT properties of the LSC were studied using the Monte Carlo ray-tracing simulation. We believed that using the approach of ray-tracing was better than that of radiative heat transfer because the latter required the spatial distribution of the energy generated inside the LSC, which was typically difficult to obtain. It would have been useful to study and understand the LSC through a simulation before the experiments were performed. The PT energy is typically from the energy loss inside the luminescent waveguide, which consists of the loss due to the relaxation energy of the luminophores and the loss due

to the photon absorbance of the host matrix. In the simulation, the LSC was configured with five layers of equal thickness, as shown in Figure 3a, and the map of the PT power of each layer was calculated. The results in Figure 3b–f indicated that the PT power was uniformly distributed in each layer. This possibly further indicated that the PT power in the LSC was one-dimensionally vertically distributed. The top layer (L1) possessed the highest PT power of 7.05 W, while the bottom layer (L5) possessed the lowest PT power of 1.08 W. This was because more photons were absorbed, and thus more PT energy was released, in the top layer than the bottom layer. The total PT power of the LSC was 13.2 W, which was much higher than the P_{max} of the LSC (1.31 W) and suggestive of a promising energy source for electric power generation in addition to the electric power from the PV conversion. Considering the PT power produced by the LSC in this study ($6.6 \times 10^4 \text{ W m}^{-3}$) was higher than that in our previous report ($6.01 \times 10^4 \text{ W m}^{-3}$) [22].

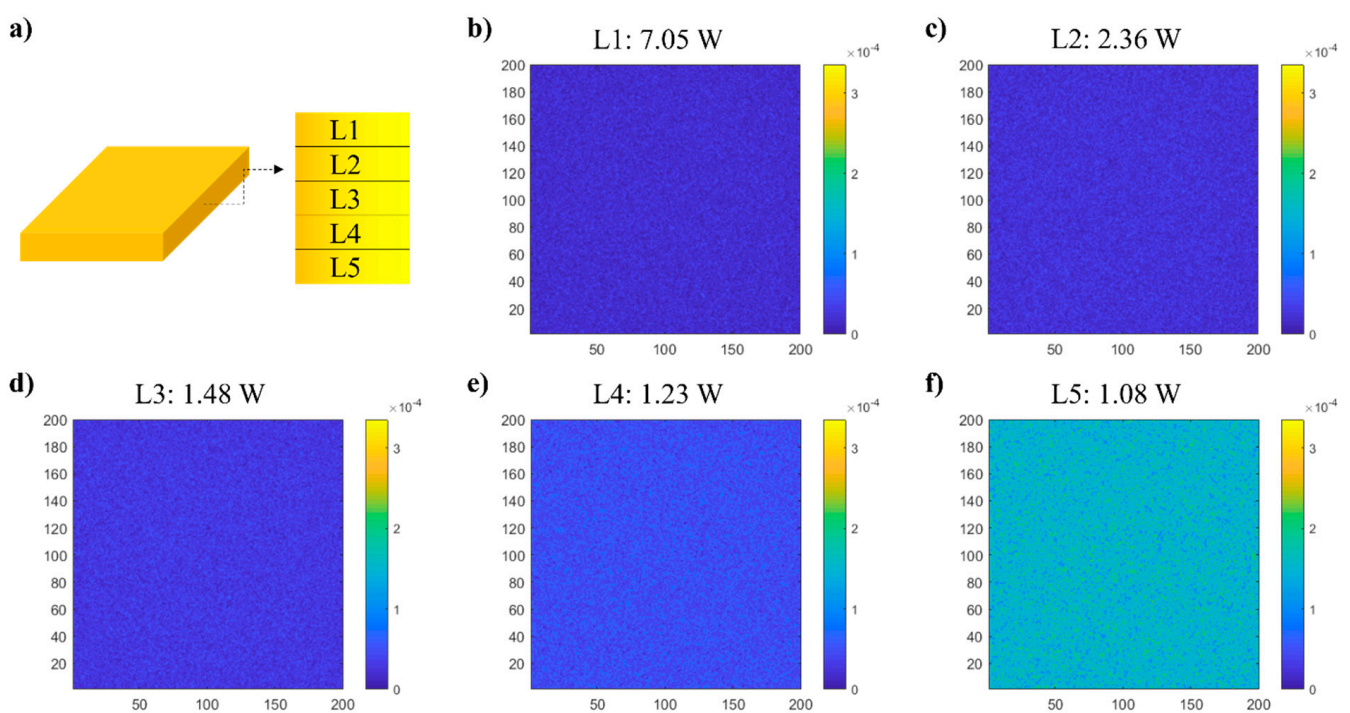


Figure 3. (a) Layer configuration of the LSC, and (b–f) heat maps of the layers (color bars with the unit of W).

3.3. Surface Heatmap

The PT energy inside the LSC should transfer to the surface of the luminescent waveguide in order to be utilized. Here, we calculated the surface heat map of the LSC. Figure 4 depicts the definition of the surface of the LSC and the surface heat map. The heat power density for each surface from 1 to 6 was 226, 226, 150, 225, 225, and 158 W m^{-2} , respectively. The results showed that the edge surfaces of the luminescent waveguide exhibited a much higher heat power density than the top and bottom surfaces. Differences at the junction of the surfaces were due to different boundary conditions that were used in the simulation. This indicated that the edge-attached solar cells would be heated during the operation of the LSC and that the performance of the solar cells would be affected. However, if the thermal energy at the edge of the luminescent waveguide was properly utilized, for example by thermoelectric devices, additional electric power could be produced by the LSC.

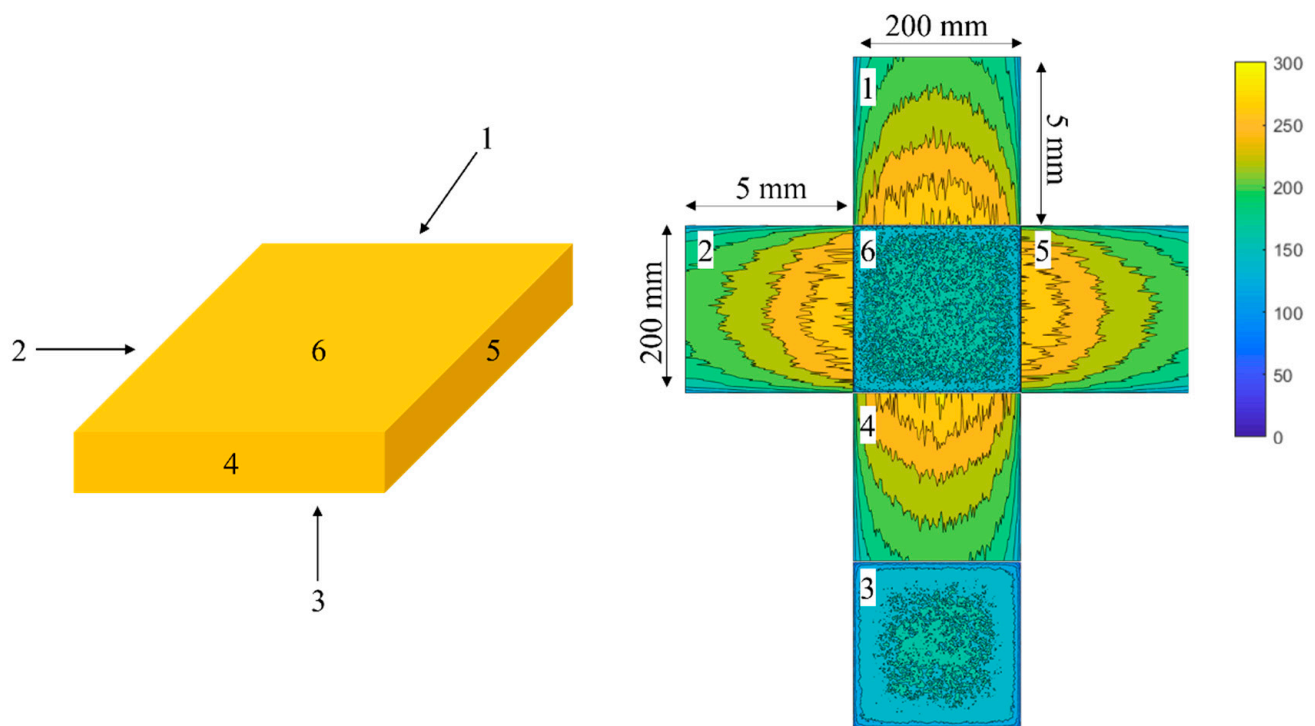


Figure 4. Surface heat map of the LSC (color bars with the unit of W m^{-2}).

4. Conclusions

In this study, we used DCJTb and GaAs solar cells to fabricate an LSC with dimensions of $200 \text{ mm} \times 200 \text{ mm} \times 5 \text{ mm}$. The PV properties of the LSC were characterized, and the device showed a PCE of 3.27% and a concentration ratio of 1.42. We performed a Monte Carlo ray-tracing simulation to investigate the PT properties of the LSC. The total PT power was 13.2 W, which was much higher than the PV power (1.31 W). The surface heat map of the LSC was further investigated, and the results revealed that the heat was concentrated on the edge of the luminescent waveguide, with a high heat power density of over 200 W m^{-2} . This suggested that the thermoelectric devices could be mounted on the edge of the luminescent waveguide associated with the solar cells to produce electricity. We believed that the results in this study would benefit the development of LSCs. The revealed PT properties provided fundamental insights for the utilization of the PT energy of LSCs. One of the direct benefits would be the improvement of the PCE of LSCs. Further work will focus on developing approaches to integrating thermoelectric devices into LSCs and on performance studies.

Author Contributions: Conceptualization, Y.L.; investigation, Y.S.; resources, Y.S.; software, Y.Z.; writing—original draft, Y.S.; writing—review & editing, Y.Z. and Y.L. All authors have read and agreed to the published version of the manuscript.

Funding: This research received no external funding.

Institutional Review Board Statement: Not applicable.

Informed Consent Statement: Not applicable.

Data Availability Statement: Not applicable.

Acknowledgments: This work is a part of the project Energy-Harvesting Windows and Panels. The authors would like to thank Solera City Energy for the research support and Solarathlon for the simulation service.

Conflicts of Interest: The authors declare no conflict of interest.

Nomenclature and Abbreviations

BIPV	building-integrated photovoltaics
DCJTb	4-(dicyanomethylene)-2- <i>tert</i> -butyl-6-(1,1,7,7-tetramethyljulolidin-4-yl-vinyl)-4 <i>H</i> -pyran
EQE	external quantum efficiency
FF	fill factor
GaAs	gallium arsenide
I_{sc}	short-circuit current
J_{sc}	short-circuit current density
LSC	luminescent solar concentrator
N_{abs}	number of absorbed photons
N_{em}	number of emitted photons
PCE	power conversion efficiency
PLQY	photoluminescence quantum yield
P_{max}	maximum electric power
PT	photothermal
PV	photovoltaic
TIR	total internal reflection
V_{oc}	open-circuit voltage

References

- Osseweijer, F.J.W.; Hurk, L.B.P.v.d.; Teunissen, E.J.H.M.; Sark, W.G.J.H.M.v. A comparative review of building integrated photovoltaics ecosystems in selected European countries. *Renew. Sustain. Energy Rev.* **2018**, *90*, 1027–1040. [\[CrossRef\]](#)
- Alim, M.A.; Tao, Z.; Hassan, M.K.; Rahman, A.; Wang, B.; Zhang, C.; Samali, B. Is it time to embrace building integrated Photovoltaics? A review with particular focus on Australia. *Sol. Energy* **2019**, *188*, 1118–1133. [\[CrossRef\]](#)
- Kuhna, T.E.; Erban, C.; Heinrich, M.; Eisenlohr, J.; Ensslen, F.; Neuhaus, D.H. Review of technological design options for building integrated photovoltaics (BIPV). *Energy Build.* **2021**, *231*, 110381. [\[CrossRef\]](#)
- Debije, M.G.; Verbunt, P.P.C. Thirty years of luminescent solar concentrator research: Solar energy for the built environment. *Adv. Energy Mater.* **2012**, *2*, 12–35. [\[CrossRef\]](#)
- Li, Y.; Zhang, X.; Zhang, Y.; Dong, R.; Luscombe, C.K. Review on the role of polymers in luminescent solar concentrators. *J. Polym. Sci. A* **2019**, *57*, 201–215. [\[CrossRef\]](#)
- Roncali, J. Luminescent solar collectors: Quo vadis? *Adv. Energy Mater.* **2020**, *10*, 2001907. [\[CrossRef\]](#)
- Zhao, Y.; Lunt, R.R. Transparent Luminescent Solar Concentrators for Large-Area Solar Windows Enabled by Massive Stokes-Shift Nanocluster Phosphors. *Adv. Energy Mater.* **2013**, *3*, 1143–1148. [\[CrossRef\]](#)
- Zhao, Y.; Meek, G.A.; Levine, B.G.; Lunt, R.R. Near-Infrared Harvesting Transparent Luminescent Solar Concentrators. *Adv. Opt. Mater.* **2014**, *2*, 606–611. [\[CrossRef\]](#)
- Yang, C.; Moemeni, M.; Bates, M.; Sheng, W.; Borhan, B.; Lunt, R.R. High-Performance Near-Infrared Harvesting Transparent Luminescent Solar Concentrators. *Adv. Opt. Mater.* **2020**, *8*, 1901536. [\[CrossRef\]](#)
- Debije, M.G.; Rajkumar, V.A. Direct versus indirect illumination of a prototype luminescent solar concentrator. *Sol. Energy* **2015**, *122*, 334–340. [\[CrossRef\]](#)
- Li, Y.; Sun, Y.; Zhang, Y. Luminescent solar concentrators performing under different light conditions. *Sol. Energy* **2019**, *188*, 1248–1255. [\[CrossRef\]](#)
- Papakonstantinou, I.; Portnoi, M.; Debije, M.G. The Hidden Potential of Luminescent Solar Concentrators. *Adv. Energy Mater.* **2021**, *11*, 2002883. [\[CrossRef\]](#)
- Slooff, L.H.; Bende, E.E.; Burgers, A.R.; Budel, T.; Pravettoni, M.; Kenny, R.P.; Dunlop, E.D.; Büchtemann, A. A luminescent solar concentrator with 7.1% power conversion efficiency. *Phys. Status Solidi RRL* **2008**, *2*, 257–259. [\[CrossRef\]](#)
- Goldschmidt, J.C.; Peters, M.; Bösch, A.; Helmers, H.; Dimroth, F.; Glunz, S.W.; Willeke, G. Increasing the efficiency of fluorescent concentrator systems. *Sol. Energy Mater. Sol. Cells* **2009**, *93*, 176–182. [\[CrossRef\]](#)
- Desmet, L.; Ras, A.J.; de Boer, D.K.; Debije, M.G. Monocrystalline silicon photovoltaic luminescent solar concentrator with 4.2% power conversion efficiency. *Opt. Lett.* **2012**, *37*, 3087–3089. [\[CrossRef\]](#) [\[PubMed\]](#)
- Li, Y.; Olsen, J.; Nunez-Ortega, K.; Dong, W.-J. A structurally modified perylene dye for efficient luminescent solar concentrators. *Sol. Energy* **2016**, *136*, 668–674. [\[CrossRef\]](#)
- Mateen, F.; Li, Y.; Saeed, M.A.; Sun, Y.; Zhang, Y.; Lee, S.Y.; Hong, S.-K. Large-area luminescent solar concentrator utilizing donor-acceptor luminophore with nearly zero reabsorption: Indoor/outdoor performance evaluation. *J. Lumin.* **2021**, *231*, 117837. [\[CrossRef\]](#)
- Li, Y.; Sun, Y.; Zhang, Y.; Li, Y.; Verduzco, R. High-performance hybrid luminescent-scattering solar concentrators based on a luminescent conjugated polymer. *Polym. Int.* **2021**, *70*, 475–482. [\[CrossRef\]](#)
- Xu, L.; Yao, Y.; Bronstein, N.D.; Li, L.; Alivisatos, A.P.; Nuzzo, R.G. Enhanced Photon Collection in Luminescent Solar Concentrators with Distributed Bragg Reflectors. *ACS Photonics* **2016**, *3*, 278–285. [\[CrossRef\]](#)

20. Fahad, M.; Oh, H.; Jung, W.; Binns, M.; Hong, S.-K. Metal nanoparticles based stack structured plasmonic luminescent solar concentrator. *Sol. Energy* **2017**, *155*, 934–941. [[CrossRef](#)]
21. Mateen, F.; Oh, H.; Kang, J.G.; Lee, S.Y.; Hong, S.-K. Improvement in the performance of luminescent solar concentrator using array of cylindrical optical fibers. *Renew. Energy* **2019**, *138*, 691–696. [[CrossRef](#)]
22. Li, Y.; Sun, Y.; Zhang, Y.; Dong, W. A Preliminary Investigation on the Photothermal Properties of Luminescent Solar Concentrators. *Optics* **2021**, *2*, 148–154. [[CrossRef](#)]
23. Alam, H.; Ramakrishna, S. A review on the enhancement of figure of merit from bulk to nano-thermoelectric materials. *Nano Energy* **2013**, *2*, 190–212. [[CrossRef](#)]
24. Twaha, S.; Zhu, J.; Yan, Y.; Li, B. A comprehensive review of thermoelectric technology: Materials, applications, modelling and performance improvement. *Renew. Sustain. Energy Rev.* **2016**, *65*, 698–726. [[CrossRef](#)]
25. Champier, D. Thermoelectric generators: A review of applications. *Energy Convers. Manag.* **2017**, *140*, 167–181. [[CrossRef](#)]
26. Li, Y.; Sun, Y.; Zhang, Y. Regional measurements to analyze large-area luminescent solar concentrators. *Renew. Energy* **2020**, *160*, 127–135. [[CrossRef](#)]
27. Li, Y.; Sun, Y.; Zhang, Y.; Dong, W.-J. Improving the photostability of printed organic photovoltaics through luminescent solar concentrators. *Opt. Mater.* **2020**, *108*, 110194. [[CrossRef](#)]
28. Li, Y.; Zhang, Y.; Sun, Y.; Ren, T. Spectral response of large-area luminescent solar concentrators. *Appl. Opt.* **2020**, *59*, 8964–8969. [[CrossRef](#)]
29. Zhao, B.; Zhang, T.; Chu, B.; Li, W.; Su, Z.; Wu, H.; Yan, X.; Jin, F.; Gao, Y.; Liu, C. Highly efficient red OLEDs using DCJTb as the dopant and delayed fluorescent exciplex as the host. *Sci. Rep.* **2015**, *5*, 10697. [[CrossRef](#)] [[PubMed](#)]
30. Kurban, M.; Gündüz, B. Physical and optical properties of DCJTb dye for OLED display applications: Experimental and theoretical investigation. *J. Mol. Struct.* **2017**, *1137*, 403–411. [[CrossRef](#)]
31. Lu, S.; Ji, L.; He, W.; Dai, P.; Yang, H.; Arimochi, M.; Yoshida, H.; Uchida, S.; Ikeda, M. High-efficiency GaAs and GaInP solar cells grown by all solid-state molecular-beam-epitaxy. *Nanoscale Res. Lett.* **2011**, *6*, 576. [[CrossRef](#)] [[PubMed](#)]
32. Libra, M.; Petrik, T.; Poulek, V.; Tyukhov, I.I.; Kouřim, P. Changes in the Efficiency of Photovoltaic Energy Conversion in Temperature Range with Extreme Limits. *IEEE J. Photovolt.* **2021**, *11*, 1479–1484. [[CrossRef](#)]
33. Debije, M.G.; Evans, R.C.; Griffini, G. Laboratory protocols for measuring and reporting the performance of luminescent solar concentrators. *Energy Environ. Sci.* **2021**, *14*, 293–301. [[CrossRef](#)]
34. Gaigalas, A.K.; Wang, L. Measurement of the Fluorescence Quantum Yield Using a Spectrometer with an Integrating Sphere Detector. *J. Res. Natl. Inst. Stand. Technol.* **2008**, *113*, 17–28. [[CrossRef](#)] [[PubMed](#)]
35. Tummeltshammer, C.; Brown, M.S.; Taylor, A.; Kenyon, A.J.; Papakonstantinou, I. Efficiency and loss mechanisms of plasmonic Luminescent Solar Concentrators. *Opt. Express* **2013**, *21*, A735–A749. [[CrossRef](#)] [[PubMed](#)]
36. Breukers, R.D.; Smith, G.J.; Stirrat, H.L.; Swanson, A.J.; Smith, T.A.; Ghigginio, K.P.; Raymond, S.G.; Winch, N.M.; Clarke, D.J.; Kay, A.J. Light losses from scattering in luminescent solar concentrator waveguides. *Appl. Opt.* **2017**, *56*, 2630–2635. [[CrossRef](#)] [[PubMed](#)]
37. Li, Y.; Sun, Y.; Zhang, Y. Boosting the cost-effectiveness of luminescent solar concentrators through subwavelength sanding treatment. *Sol. Energy* **2020**, *198*, 151–159. [[CrossRef](#)]